




Transport-induced-charge electroosmosis in nanoporesWei-Lun Hsu ^{1,*}, Zhixuan Wang,¹ Soumyadeep Paul ^{1,2} and Hirofumi Daiguji ¹¹*Department of Mechanical Engineering, The University of Tokyo, Bunkyo-ku, Tokyo 113-8656, Japan*²*Department of Mechanical Engineering, Stanford University, Stanford, California 94305, USA*

(Received 31 July 2021; accepted 7 May 2024; published 2 July 2024)

We obtain analytical solutions for transport-induced-charge electroosmosis (TICEO) in a nanopore under steady-state and transient conditions, when the applied salt concentration difference Δn_0 is much smaller than the average salt concentration n_0 under a moderate applied electric field \mathbf{E} . The TICEO velocity in an uncharged pore is found to be proportional to $|\mathbf{E}|^2$ and the concentration gradient ∇n_0 . For charged pores, we define a dimensionless parameter ξ , where TICEO governs the electroosmotic behavior over conventional electroosmosis attributed from electric double layers when $\xi \gg 1$, resulting in a net electroosmotic flow independent of the surface charge, making it suitable for alternating current (ac) pumping applications. Moreover, we estimate the characteristic time τ of TICEO development to be on the order of tens of picoseconds for a 1 M potassium chloride aqueous solution, which suggests that ac nanopore pumping using TICEO can be effective up to gigahertz frequency. Significantly, it is indicated that the maximum pumping flow rate can be achieved at an optimal pore aspect ratio $\chi_c = 0.457$, providing important information to future experimental designs.

DOI: [10.1103/PhysRevFluids.9.L071701](https://doi.org/10.1103/PhysRevFluids.9.L071701)

In the past two decades, the advent of nanometer-sized pore milling techniques using transmission electron microscopy and electron-beam lithography [1,2] has shifted the dimensions of interest in electrokinetic phenomena from the microscale to nanoscale [3,4]. In particular, the emergence of low aspect ratio (pore length/pore diameter) nanopores offers tremendous potential for high precision biosensing for rapid medical diagnosis and high-power-density energy conversion [5,6]. When an electric field is imposed across a nanopore, a salt gradient coexists in many cases [7,8]. For instance, Wanunu *et al.* demonstrated that the addition of a salt concentration bias across nanopores leads to enhanced DNA sensing efficiency [9]. A local concentration difference may also arise across an ion selective membrane due to the ion concentration polarization phenomenon [10]. In this regard, the nonuniform electric field caused by the salt gradient gives rise to local ion separation in electrolyte solutions with a thin membrane, known as the transport-induced-charge (TIC) phenomenon [11–13]. The TIC phenomenon yields unique electroosmotic behavior that is distinct from the classical Helmholtz-Smoluchowski flow, arising from the electric force on the charged solution within the electric double layer (EDL). From a fundamental perspective, these two charge types are disparate in that ion separation due to a salt gradient only occurs in nonequilibrium conditions when an electric field is applied, whereas the interfacial charges within the EDL exist with or without an external electric field.

Previous studies have found unique electrokinetic behavior as TIC occurs. He *et al.* indicated that the induced charges near the entrance of a nanopore might facilitate the capture of DNA molecules for resistive pulse sensing [14]. In nanochannels, Zhu *et al.* pointed out that locally

*Contact author: wlsu@thml.t.u-tokyo.ac.jp

induced charges yield inverse screening effects by coions, giving rise to local vortices [15]. Different from conventional electrokinetic phenomena, such as EDL electroosmosis [3], diffusioosmosis [16–19], and electrodiffusioosmosis [20–22], occurring in the vicinity of a charged solid, Hsu *et al.* [13] indicated that the TIC does not originate from the charges in the EDL, and thus can be generated even in uncharged pores. Due to the interwoven effects of a local electric field and a salt concentration gradient, the solution conductivity variation renders unequal conduction current fluxes across the nanopore and thus disparate diffusion fluxes of ions occur, resulting in local ion separation. Interestingly, Hsu *et al.* found that the induced charges were inverted when the external electric field direction was reversed, resulting in a unidirectional flow in a neutral nanopore independent of the direction of the imposed electric field [13]. This led to a novel concept of alternating current (ac) nanopore resistive pulse sensing. To distinguish the flow from the induced-charge electroosmosis (ICEO) in microfluidic systems generated around a polarized metallic or dielectric material [23,24], the term “transport-induced-charge electroosmosis” (TICEO) was introduced [13]. Note that despite a similar expression, TICEO and ICEO are different electrokinetic phenomena. In particular, TICEO is an electrokinetic phenomenon caused by the local ion separation in the liquid, while the latter occurs near a polarizable material, due to the polarized charge on the solid surface, forming an induced EDL. In contrast to ICEO, which has been extensively utilized in microfluidic ac pumping, there is no requirement for metal patches in the case of TICEO, significantly simplifying the fabrication process allowing the applicable length scale for nanofluidic ac pumping down to sub-100 nm.

Despite previous numerical investigations of the TIC phenomenon, there are no analytical expressions for quantitative description of TICEO and its influence on the overall electroosmotic behavior, greatly impeding our understanding of the flow behavior. In this study, we construct a simple analytical model and investigate suitable operating conditions of TICEO in nanopores in the presence of an external electric field and a salt concentration difference. The investigated system is illustrated in Fig. 1(a). The considered pore geometry is cylindrical with a typical radius R of 2.5 nm and a length L of 20 nm. A monovalent aqueous electrolyte solution of the average bulk concentration $n_0 = 1$ M is filled while an external salt concentration difference Δn_0 and an electric potential difference $\Delta\psi$ across the two ends of the pore are simultaneously imposed. The analytical results are compared with numerical simulation modeling detailed in Supplemental Material S1 [25], including Refs. [13,26–31]. Using the constructed analytical model, the time scale, length scale, and typical voltage ranges for the occurrence of TICEO in a salt-concentration-biased nanopore are clarified.

We begin the analysis by considering ion conservation. Ion transport in a nanopore obeys the conservation of current density derived from the charge conservation equation:

$$\frac{\partial \rho_e}{\partial t} = -\nabla \cdot \mathbf{J}, \quad (1)$$

where ρ_e , t , and \mathbf{J} denote the space charge density, time, and current density, respectively. We consider a small salt concentration perturbation where Δn_0 is much lower than n_0 . In such a condition, the current density \mathbf{J} can be estimated by Ohm’s Law using the bulk solution conductivity σ_c , i.e., $\mathbf{J} \cong \sigma_c \mathbf{E}$, implying that both the diffusion current and the advection current are negligible compared with the magnitude of the conduction current [32]. Here, the electric field \mathbf{E} equals the sum of the electric field in absence of the concentration difference \mathbf{E}_0 and the perturbed electric field due to the presence of the concentration difference $\delta\mathbf{E}$, i.e., $\mathbf{E} = \mathbf{E}_0 + \delta\mathbf{E}$. Note that this Ohmic assumption is valid under a small salt concentration variation across the nanopore when $\Delta n_0 \ll n_0$, although the numerical simulation indicates that the Ohmic behavior remains up to a moderate concentration difference when $\Delta n_0/n_0 \leq 0.3$ (see Supplemental Material S2 for details [25], including Ref. [33]). Based on Gauss’s law, the relation between \mathbf{E} and ρ_e can be described:

$$\nabla \cdot (\varepsilon_0 \varepsilon \mathbf{E}) = \rho_e, \quad (2)$$

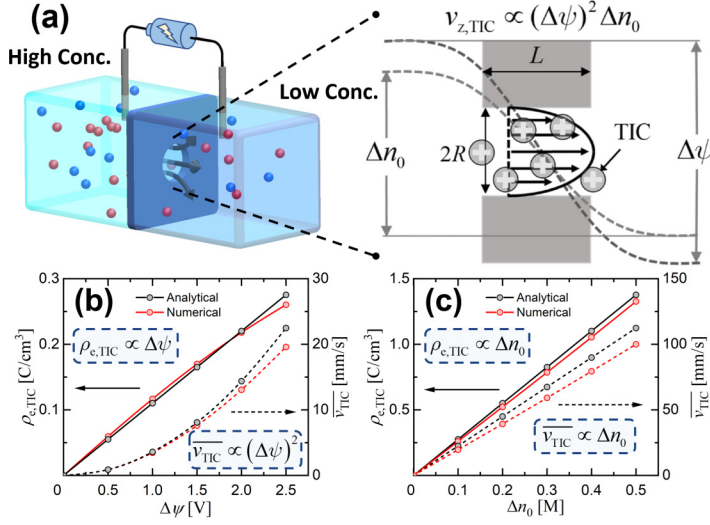


FIG. 1. (a) Schematic illustration of transport-induced-charge (TIC) electroosmotic velocity $v_{z,\text{TIC}}$ distribution in an uncharged nanopore when an electric potential bias $\Delta\psi$ and a salt concentration difference Δn_0 are concurrently imposed (where the dark-gray and light-gray dashed curves indicate the electric potential and concentration variations, respectively). $v_{z,\text{TIC}}$, L , and R are the TIC velocity, pore length, and pore radius, respectively. (b), (c) Comparisons between analytical solutions (black curves) and numerical simulation results (red curves) for the steady-state TIC density $\rho_{e,\text{TIC}}$ (solid curves) and mean TIC electroosmotic velocity \bar{v}_{TIC} (dashed curves) in a nanopore with the length $L = 20$ nm and radius $R = 2.5$ nm, $n_0 = 1$ M, where (b) $\Delta n_0 = 0.1$ M for different $\Delta\psi$ and (c) $\Delta\psi = 2.5$ V for different Δn_0 . (The simulated values of $\rho_{e,\text{TIC}}$ and \bar{v}_{TIC} are derived from the average values on the cross-sectional area in the middle of the pore.)

where ε_0 is the permittivity in a vacuum and ε the dielectric constant. Equation (2) becomes Poisson's equation when expressing \mathbf{E} in terms of electric potential ψ (i.e., $\mathbf{E} = -\nabla\psi$).

In the following, we separately investigate steady-state TIC electroosmotic flow (EOF) and transient TIC EOF, including either a constant applied electric potential difference or an alternating current field. Substituting Eq. (2) into Eq. (1) at $\partial\rho_e/\partial t = 0$, the steady-state charge distribution in the solution is obtained as [34]

$$\rho_e = \varepsilon_0 \varepsilon \mathbf{E} \cdot \left(\frac{\nabla \varepsilon}{\varepsilon} - \frac{\nabla \sigma_c}{\sigma_c} \right). \quad (3)$$

Because both ε and σ_c are temperature dependent, TIC can also be generated under a temperature gradient according to this equation, which is known as electrothermal effects [35]. In a similar vein, the TIC phenomenon can occur at the junction of two solutions with asymmetric viscosity or permittivity, as long as a nonuniform conductivity or permittivity field exists (in addition to the applied electric field). Owing to the small concentration perturbation, we assume a linear distribution of the salt concentration along the axial direction in the nanopore without a permittivity gradient (see Supplemental Material S3 for justification [25], including Ref. [42]), when Joule heating is negligible. In combination with the assumption of equal ionic diffusivities between cations and anions [such as potassium chloride (KCl) solutions], the steady-state TIC charge density $\rho_{e,\text{TIC}}$ can be approximated as

$$\rho_{e,\text{TIC}} = -\frac{\varepsilon_0 \varepsilon E_{\text{pore}}}{L} \left(\frac{\Delta n_{0,\text{pore}}}{n_0} \right), \quad (4)$$

where E_{pore} and $\Delta n_{0,\text{pore}}$ denote the axial electric field in the nanopore and salt concentration difference across the nanopore, respectively. Note that owing to the external electric field and circuit,

there exists a net ionic current in the system, implying the influence of asymmetric ionic diffusivity, which is ignored here, will differ from the electroosmotic effect in diffusioosmosis under an open circuit condition [17].

Attributed to the small concentration perturbation, we consider $\delta\mathbf{E} \ll \mathbf{E}_0$ and thus a constant electric field in the nanopore $E_{\text{pore}} \cong E_{\text{pore},0}$ is taken into account, where $E_{\text{pore},0}$ is the axial electric field in the nanopore in absence of the concentration difference. We employ Hall's form of access resistance, where the electric potential drops are analyzed by a circuit model [36]. When $\Delta n_0 \ll n_0$, the variation of σ_c between the reservoirs is negligible. Thus, the net resistance is equal to the sum of the pore resistance $R_{\text{pore}} = \frac{L}{\sigma_c \pi R^2}$ and the access resistance $R_{\text{access}} = \frac{1}{2\sigma_c R}$ at the junctions of the nanopore and reservoirs. Consequently, E_{pore} can be expressed as a function of the external electric potential difference $\Delta\psi$ as [37,38]

$$E_{\text{pore}} \cong E_{\text{pore},0} = -\frac{2\Delta\psi}{\pi R + 2L}. \quad (5)$$

This implies that the induced charge distribution is uniform in the nanopore under a small concentration difference as indicated by Eq. (4), which is close to previous numerical results [13]. On the other hand, an additional condition is required to acquire the concentration variation in the nanopore [39]. We consider that at the junctions between the nanopore and reservoirs, $\rho_{e,\text{TIC}}$ inside the pore is close to that within the hemispherical access regions. This results in a constant product of the potential drop and concentration difference within each region, yielding

$$\Delta n_{0,\text{pore}} = \frac{\pi L \Delta n_0}{8R + \pi L}, \quad (6)$$

where $\Delta n_{0,\text{access}} = \Delta n_0 - \Delta n_{0,\text{pore}}$ is the concentration difference within the hemispherical access regions (see Supplemental Material S4 for details [25], including Refs. [36,40]).

The electroosmotic velocity in the axial (z) direction $v_z(r)$ can be described by the Navier-Stokes equation:

$$\eta \frac{1}{r} \frac{d}{dr} \left(r \frac{dv_z(r)}{dr} \right) + \rho_e E_{\text{pore}} = 0, \quad (7)$$

where the dynamic viscosity η is assumed as constant when the viscoelectric effect is insignificant at low surface charge densities [41], and r is the radial coordinate. Equation (7) assumes that the inertia force and pressure difference arising from the pore boundary effects at the inlet and outlet are small. The TIC EOF is driven by the electric force acting on the TIC, and its velocity profile $v_{z,\text{TIC}}(r)$ follows a parabolic distribution:

$$v_{z,\text{TIC}}(r) = -\frac{\varepsilon_0 \varepsilon R^2 E_{\text{pore}}^2}{4\eta L} \left(\frac{\Delta n_{0,\text{pore}}}{n_0} \right) \left[1 - \left(\frac{r}{R} \right)^2 \right]. \quad (8)$$

As a result, the mean TIC electroosmotic velocity $\overline{v_{\text{TIC}}}$ becomes

$$\overline{v_{\text{TIC}}} = -\frac{\varepsilon_0 \varepsilon R^2 E_{\text{pore}}^2}{8\eta L} \left(\frac{\Delta n_{0,\text{pore}}}{n_0} \right). \quad (9)$$

For verification, we conduct numerical simulations using the coupled Poisson-Nernst-Planck (including the advection and diffusion terms), Navier-Stokes (including the inertia and pressure terms), and continuity equations (detailed in Supplemental Material S1 [25], including Refs. [26–29]). The analytical solutions and numerical results at steady state are compared in Figs. 1(b) and 1(c), showing close agreement for both $\rho_{e,\text{TIC}}$ and $\overline{v_{\text{TIC}}}$. It is worth highlighting that although the model is constructed under the low Δn_0 and linear concentration distribution in the nanopore (which is valid when $\Delta\psi$ is small), the typical errors are less than 5% for $\rho_{e,\text{TIC}}$ and less than 10% for $\overline{v_{\text{TIC}}}$ even at relatively high $\Delta\psi = 2.5$ V and $\Delta n_0 = 0.5$ M. The errors decrease as $\Delta\psi$ and Δn_0 decrease, indicating that the assumption made in Eq. (7) is valid within the investigated ranges of parameters; that is, the velocity change due to the pressure drop induced across the nanopore is negligible

compared with $\overline{v_{\text{TIC}}}$ according to the numerical simulation results (see Supplemental Material S5 for justification [25], including Refs. [33]). The simulation results suggest that $\rho_{e,\text{TIC}} \propto \Delta\psi \Delta n_0$ and $\overline{v_{\text{TIC}}} \propto (\Delta\psi)^2 \Delta n_0$ following Eqs. (4) and (9). The deviations between the analytical model and numerical simulation results at high $\Delta\psi$ and Δn_0 are primarily due to the decreased apparent concentration difference in the pore and the polarization of the TIC, respectively. A detailed analysis can be found in Supplemental Material S3 [25], including Ref. [42]. The electric field magnitude in the pore $|E_{\text{pore}}|$ is between 4.18×10^6 and 1.04×10^8 V/m for $0.1 \text{ V} \leq \Delta\psi \leq 2.5 \text{ V}$, close to previous experimental systems [43,44] [estimated by Eq. (5)]. Despite the large electric field, previous molecular dynamics studies have shown that the ions remain fully hydrated even under a higher electric field magnitude at 10^9 V/m [45,46], justifying the present model.

The analysis so far is based on an uncharged nanopore for an ideal case; in practical systems, the EDL at the liquid-solid interface can yield significant effects on electroosmotic behavior in addition to the TIC EOF. To suppress the EDL EOF, which largely depends on the surface charge property, a solution pH near the material's isoelectric point should be selected, or operating conditions in which the TIC EOF is dominant must be employed. To demonstrate the latter, we incorporate the effects of surface charge and examine the competition between the EDL EOF and TIC EOF in a charged nanopore of which the Debye length λ_D is thin compared with the pore radius R for high salt concentrations, rendering the Dukhin number, Du , much less than 1 [26]. The EDL EOF velocity profile $v_{z,\text{EDL}}(r)$ in a cylindrical pore in the absence of an external pressure gradient can be expressed as [26]

$$v_{z,\text{EDL}}(r) = -\frac{\varepsilon_0 \varepsilon \zeta E_{\text{pore}}}{\eta} \left[1 - \frac{I_0(\kappa r)}{I_0(\kappa R)} \right], \quad (10)$$

where ζ is the zeta potential, κ the reciprocal of the Debye length, and I_0 the zeroth-order modified Bessel function of the first kind. The mean EDL electroosmotic velocity $\overline{v_{\text{EDL}}}$ can be obtained as

$$\overline{v_{\text{EDL}}} = -\frac{\varepsilon_0 \varepsilon \zeta E_{\text{pore}}}{\eta} \left[1 - \frac{2}{\kappa R} \frac{I_1(\kappa R)}{I_0(\kappa R)} \right], \quad (11)$$

where I_1 is the first-order modified Bessel function of the first kind [47]. The net EOF comes from the electric force acting on both the charges of the EDL and the TIC. By considering a linear combination of these two effects, viz., $v_z(r) = v_{z,\text{TIC}}(r) + v_{z,\text{EDL}}(r)$ (a similar superposition approach has been adopted in other systems [24,48]), the mean electroosmotic velocity $\overline{v} = \overline{v_{\text{TIC}}} + \overline{v_{\text{EDL}}}$ can be derived as

$$\overline{v} = -\frac{\varepsilon_0 \varepsilon}{\eta} \left\{ \frac{R^2 E_{\text{pore}}^2}{8L} \left(\frac{\Delta n_{0,\text{pore}}}{n_0} \right) + \zeta E_{\text{pore}} \left[1 - \frac{2}{\kappa R} \frac{I_1(\kappa R)}{I_0(\kappa R)} \right] \right\}. \quad (12)$$

In this equation, the first-order term of E_{pore} comes from the EOF due to the charges in the EDL, while the quadratic term is attributed by the TIC in the solution throughout the nanopore. There exhibits a reinforcement or competition between the EDL electroosmosis and TIC electroosmosis according to their directions. When the TIC has the opposite sign to the counterions of the charged surface, there is competition between the EDL EOF and the TIC EOF. For better control of the flow behavior, we define a dimensionless number $\xi = \overline{v_{\text{TIC}}}/\overline{v_{\text{EDL}}}$ to evaluate the dominant source of the EOF:

$$\xi = -\frac{R^2 E_{\text{pore}}}{8L\zeta} \left(\frac{\Delta n_{0,\text{pore}}}{n_0} \right) \left[1 - \frac{2}{\kappa R} \frac{I_1(\kappa R)}{I_0(\kappa R)} \right]^{-1}, \quad (13)$$

where $\xi = 1$ when $\overline{v} = 0$. Hence, when $\xi \ll 1$, the EDL EOF is dominant, whereas when $\xi \gg 1$, the TIC EOF governs the flow behavior at high applied voltages.

The electroosmotic behavior in a nanopore is schematically illustrated in Fig. 2(a), which shows a negatively charged surface with negative TIC, implying that \mathbf{E} and ∇n_0 are in the same direction. In this case, the velocities generated by EDL EOF and TIC EOF in the pore oppose each other. Note

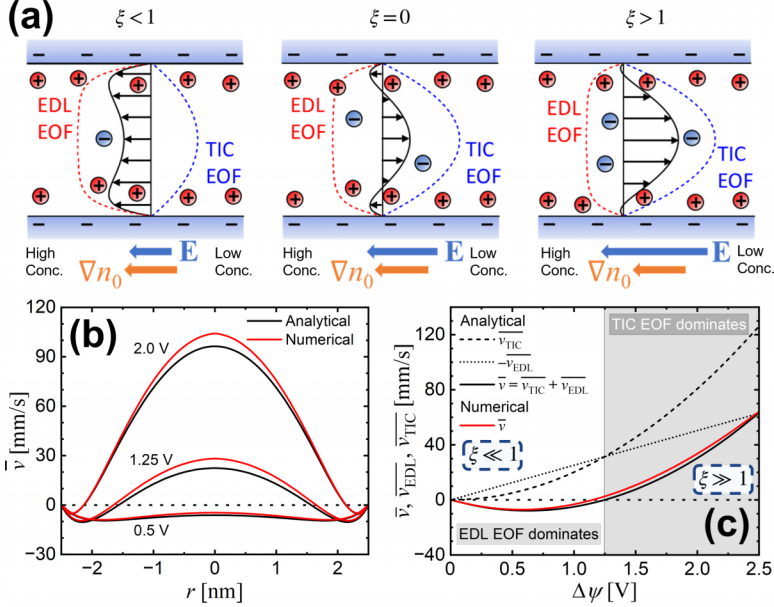


FIG. 2. (a) Schematic illustration of the electroosmotic flow (EOF) behavior in a charged nanopore, depicting the competition between the electric double layer (EDL) EOF and the TIC EOF with respect to the dimensionless number ξ . (b) Steady-state electroosmotic velocity profiles $v_z(r) = v_{z,\text{TIC}}(r) + v_{z,\text{EDL}}(r)$ in the pore at voltages of 0.5 V ($\xi < 1$), 1.25 V ($\xi = 1$), and 2 V ($\xi > 1$). (c) Variations of steady-state mean electroosmotic velocity \bar{v} and its velocity components \bar{v}_{EDL} and \bar{v}_{TIC} from EDL EOF and TIC EOF, respectively, as a function of the applied electric field $\Delta\psi$. [For (b) and (c), $n_0 = 1$ M, $\Delta n_0 = 0.5$ M, $\zeta = -1$ mV, $L = 20$ nm, and $R = 2.5$ nm.]

that $\lambda_D \cong 0.3$ nm at $n_0 = 1$ M for KCl solutions is much smaller than $R = 2.5$ nm. Hence, the EDL EOF is close to uniform near the axis. The transition of the velocity profile from low to high ξ is shown in Fig. 2(b). Figure 2(c) shows the variation of \bar{v} and its velocity components. The numerical results are consistent with the analytical solution, verifying the linear superposition assumption in Eq. (12). For $\xi \ll 1$, the EDL EOF is dominant, yielding a unidirectional EOF distribution in spite of the concave velocity profile near the axis. For $\xi = 1$, the net flow rate of EDL EOF is balanced by that of TIC EOF. It is worth emphasizing that the TIC charge density (-0.7 C/cm³) is still much lower than the space charge density from the EDL in the vicinity of the surface (6.8 C/cm³), implying that the presence of TIC does not substantially distort the charge distribution from EDL. However, the no-slip surface remarkably suppresses the development of the EDL EOF, while having less impact on the parabolic TIC EOF. For $\xi \gg 1$, the TIC EOF is dominant, and the velocity profile becomes close to parabolic.

Prior to the analysis of ac electrokinetic pumping, we investigate the transient variation of induced charge $\rho_{e,\text{TIC}}^*(t)$ at a fixed external potential difference $\Delta\psi$. Considering the case where ε is constant and $\rho_{e,\text{TIC}}^*(t)$ is uniform in the nanopore, we derive a first-order differential equation for $\rho_{e,\text{TIC}}^*(t)$ from Eqs. (1) and (2):

$$\frac{d\rho_{e,\text{TIC}}^*(t)}{dt} + \frac{\sigma_c}{\varepsilon_0\varepsilon}\rho_{e,\text{TIC}}^*(t) = -\frac{\sigma_c E_{\text{pore}}}{L} \left(\frac{\Delta n_{0,\text{pore}}}{n_0} \right). \quad (14)$$

Equation (14) is solved under the initial condition that $\rho_{e,\text{TIC}}^*(0) = 0$, implying no induced charge when the electric field is absent. Increasing the electric field in a step from 0 to E_{pore} at $t = 0$, we

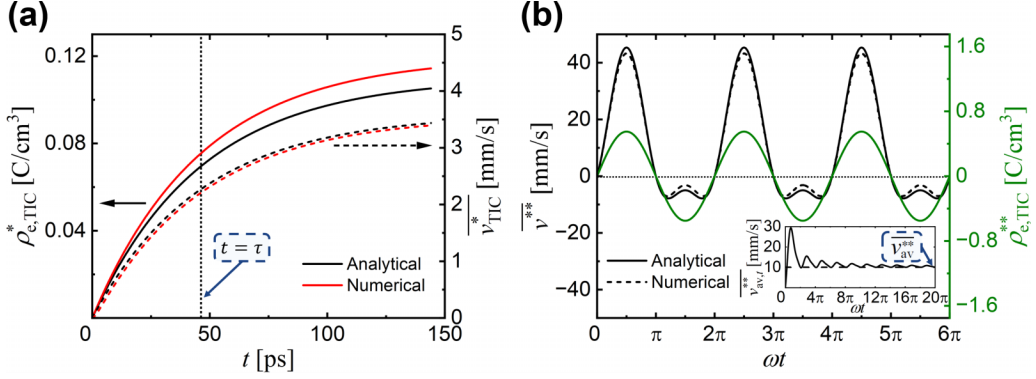


FIG. 3. (a) Comparisons between the analytical solutions (black curves) and numerical simulation results (red curves) of the transient TIC density $\rho_{e,TIC}^*$ (solid curves) and mean TIC electroosmotic velocity \overline{v}_{TIC}^* (dashed curves) in a nanopore at $\Delta n_0 = 0.1$ M and $\Delta\psi = 1$ V, where τ is the characteristic time $\cong 46.3$ ps derived from Eq. (16). (b) Analytical solution (solid curves) and numerical simulation results (dashed curve) of the mean ac flow velocity \overline{v}^{**} (black curves) and the ac induced charge density $\rho_{e,TIC}^{**}$ (green curve) at $\zeta = -1$ mV with respect to the dimensionless time (ωt) at $\alpha = 1$ V, $\Delta n_0 = 0.5$ M, and $\nu = 100$ kHz. The inset shows the simulation results of the time-averaged mean ac flow velocity $\overline{v}_{av,t}^{**}$, where \overline{v}_{av}^{**} is the time-averaged mean electroosmotic velocity during each period when it approaches a constant. Other parameters are $n_0 = 1$ M, $L = 20$ nm, and $R = 2.5$ nm.

derive the transient variation of $\rho_{e,TIC}^*(t)$ as the following relaxation expression:

$$\rho_{e,TIC}^*(t) = -\frac{\varepsilon_0 \varepsilon E_{\text{pore}}}{L} \left(\frac{\Delta n_{0,\text{pore}}}{n_0} \right) (1 - e^{-t/\tau}), \quad (15)$$

where, for monovalent electrolytes, the characteristic time τ is

$$\tau = \frac{\varepsilon_0 \varepsilon}{\sigma_c} = \frac{\varepsilon_0 \varepsilon k_B T}{2e^2 n_0 \overline{D}}, \quad (16)$$

where k_B , T , e , and \overline{D} are the Boltzmann's constant, temperature, element charge, and arithmetic mean ionic diffusivity, respectively. Hence, the transient TIC electroosmotic velocity $v_{TIC}^*(r, t)$ in a circular channel and the corresponding transient mean TIC electroosmotic velocity $\overline{v}_{TIC}^*(t)$ can be derived by assuming a quasi-steady-state response to $\rho_{e,TIC}^*(t)$ in the flow behavior, because the diffusion of ions is much slower than the diffusion of fluid vorticity (by a factor of $\sim 10^{-3} \cong \overline{D}/\nu_f$, where $\nu_f = \eta/\rho$ is the kinematic viscosity and ρ the solution density):

$$v_{TIC}^*(r, t) = \rho_{e,TIC}^*(t) \frac{R^2 E_{\text{pore}}}{4\eta} \left[1 - \left(\frac{r}{R} \right)^2 \right], \quad (17)$$

$$\overline{v}_{TIC}^*(t) = -\frac{\varepsilon_0 \varepsilon R^2 E_{\text{pore}}^2}{8\eta L} \left(\frac{\Delta n_{0,\text{pore}}}{n_0} \right) (1 - e^{-t/\tau}). \quad (18)$$

Figure 3(a) shows that there is good agreement between the analytical and numerical solutions for the transient variations of $\rho_{e,TIC}^*(t)$ and $\overline{v}_{TIC}^*(t)$. τ is derived as $\cong 46.3$ ps for KCl solutions at $n_0 = 1$ M and $T = 298$ K, where the charge induction process reaches steady state in $\cong 100$ ps. The momentum balance equation gives a time scale of $\tau_{\nu,f} = R^2/\nu_f$ for the diffusion of fluid vorticity due to viscosity [24]. For a nanopore with a radius of 2.5 nm, $\tau_{\nu,f} = 1.6$ ps, which is one order of magnitude smaller than τ , indicating that the redistribution of ions is the time-determining step for the development of TIC EOF.

Under an ac field, where the applied electric potential difference $\Delta\psi_{ac}(t) = \alpha \sin(2\pi\nu t)$ is a sinusoidal function of the amplitude α and frequency ν , the ac induced charge density $\rho_{e,TIC}^{**}(t)$ follows Eq. (14):

$$\frac{d\rho_{e,TIC}^{**}(t)}{dt} + \beta\rho_{e,TIC}^{**}(t) = \gamma\Delta\psi_{ac}(t). \quad (19)$$

In these expressions, $\beta = 1/\tau$ and $\gamma = \frac{2\sigma_c}{(\pi R + 2L)L} \left(\frac{\Delta n_{0,pore}}{n_0}\right)$. Using the initial condition that $\rho_{e,TIC}^{**}(0) = 0$, $\rho_{e,TIC}^{**}(t)$ can be solved as

$$\rho_{e,TIC}^{**}(t) = \frac{\alpha\beta\gamma \sin(\omega t) - \alpha\gamma\omega[\cos(\omega t) - e^{-\beta t}]}{\beta^2 + \omega^2}, \quad (20)$$

where $\omega = 2\pi\nu$. Accordingly, the mean ac flow velocity $\overline{v^{**}}(t)$ has contributions from both EDL EOF and TIC EOF, and can be expressed as

$$\overline{v^{**}}(t) = \frac{2\Delta\psi_{ac}(t)}{\pi R + 2L} \left\{ -\frac{\rho_{e,TIC}^{**}(t)R^2}{8\eta} + \frac{\varepsilon_0\varepsilon\xi}{\eta} \left[1 - \frac{2}{\kappa R} \frac{I_1(\kappa R)}{I_0(\kappa R)} \right] \right\}. \quad (21)$$

Typical behaviors of $\rho_{e,TIC}^{**}(t)$ and $\overline{v^{**}}(t)$ under an ac field are shown in Fig. 3(b) (taking positive values as the TIC EOF direction). Given that $\xi \cong 0.8 < 1$ when $\Delta\psi_{ac} = 1$ V in this case, the EDL EOF is dominant as $\rho_{e,TIC}^{**}(t) < 0$, resulting in a negative velocity. Both the EDL EOF and the TIC EOF are in the positive direction when $\rho_{e,TIC}^{**}(t) > 0$, giving rise to an obvious rectification of $\overline{v^{**}}(t)$ between the different voltage directions. The inset of Fig. 3(b) shows the time-averaged mean ac flow velocity $\overline{v_{av,t}^{**}} = \frac{1}{t} \int_0^t \overline{v^{**}}(t) dt$, which approaches a stable value in a few cycles, yielding a net flow in the same direction under an ac field.

Accordingly, we investigate suitable time and length scales for ac electrokinetic pumping using TICEO in nanopores. When the flow reaches an approximate statistical steady state, the time-averaged mean electroosmotic velocity $\overline{v_{av}^{**}}$ during each period $1/\nu$ can be derived by integrating $\overline{v^{**}}(t)$ over time:

$$\begin{aligned} \overline{v_{av}^{**}} &= \nu \int_0^{1/\nu} \overline{v^{**}}(t) dt \\ &= \frac{\alpha^2\beta\gamma R^2}{8\eta(\beta^2 + \omega^2)(\pi R + 2L)} [\neq f(\xi)] \\ &\cong \frac{\alpha^2\gamma R^2}{8\eta\beta(\pi R + 2L)}, \quad \text{when } \omega \ll \beta. \end{aligned} \quad (22)$$

Importantly, the net zero contribution from the EDL EOF for each cycle means that $\overline{v_{av}^{**}}$, which is proportional to α^2 , is independent of ζ , regardless of the magnitude of ξ . The variation of $\overline{v_{av}^{**}}$ as a function of the pore aspect ratio $\chi = L/D$, where $D = 2R$ is the pore diameter, is shown in Fig. 4. For a fixed R , $\overline{v_{av}^{**}}$ increases monotonically for a shorter L (black curves). Conversely, $\overline{v_{av}^{**}}$ attains a maximum value when the first derivative of $\overline{v_{av}^{**}}$ with respect to χ is zero as χ increases at a fixed L (green curves). This occurs when χ is equivalent to a critical value χ_c :

$$\chi_c = \frac{\sqrt{1 + \pi^2/2} - 1}{\pi} \cong 0.457. \quad (23)$$

Although the numerical simulation shows that the zero pressure gradient assumption becomes invalid for ultrathin nanopores when $\chi < 2$, the maximum TIC EOF appears as χ approaches approximately 0.5 close to the prediction from Eq. (23) (see Supplemental Material S5 for details, including Ref. [49]). Thus, the maximum flow rate per unit area can be achieved using low-aspect-ratio pores whose length and radius are similar. On the other hand, when the angular frequency of the ac field is much smaller than $1/\tau$, the time-averaged mean flow velocity can be regarded as a

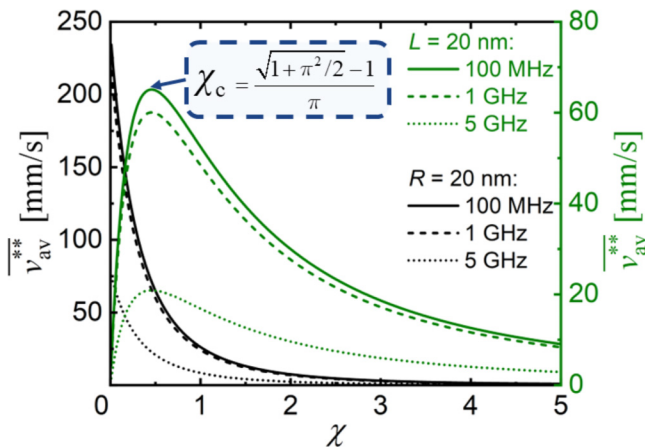


FIG. 4. Variation of time-averaged mean electroosmotic velocity $\overline{v_{av}^{**}}$ over each period $1/\nu$ under an ac sinusoidal field as a function of the pore aspect ratio $\chi = L/D$ at different frequencies ν when $\alpha = 2.5$ V, $n_0 = 1$ M, and $\Delta n_0 = 0.1$ M. L and $R (=D/2)$ are fixed at 20 nm for the green and black curves, respectively. The optimized pore aspect ratio χ_c can be obtained from Eq. (23).

constant and is independent of the frequency. At $n_0 = 1$ M, $\beta/2\pi$ is approximately 3.4×10^9 Hz. Therefore, $\overline{v_{av}^{**}}$ is independent of the frequency when $\nu \ll 1$ GHz.

In summary, we have analytically investigated TICEO for three cases: (i) the steady state, (ii) transient variations under a constant applied voltage, and (iii) transient variations under a sinusoidal ac field. The analytical results are in good agreement with the numerical simulations. We defined a dimensionless number ξ to evaluate the dominance of TICEO [Eq. (13)]. When $\xi \gg 1$, TIC EOF is dominant over EDL EOF, allowing for a unidirectional flow. Under an ac field, a net unidirectional flow occurs, regardless of ξ . Furthermore, we obtained the characteristic time τ [Eq. (16)] for the TIC phenomenon, which is on the order of tens of picoseconds for 1 M KCl electrolytes, allowing for pumping applications with a high frequency up to the gigahertz level. Finally, the optimal pore aspect ratio χ_c was determined [Eq. (23)], which shows that the largest mean electroosmotic velocity under a sinusoidal ac field occurs when $L \cong 0.457D$. These results provide direct guidance for the nanopore design of ac pumping, paving the way for precise flow control in nanopores.

The authors thank Juan G. Santiago and Ali Mani at Stanford University, as well as Jongyoon Han and Rohit Karnik at Massachusetts Institute of Technology, for their comments. This work was supported by JSPS KAKENHI Grant No. JP19K15600.

-
- [1] A. J. Storm, J. H. Chen, X. S. Ling, H. W. Zandbergen, and C. Dekker, Fabrication of solid-state nanopores with single-nanometre precision, *Nat. Mater.* **2**, 537 (2003).
 - [2] D. V. Verschueren, W. Yang, and C. Dekker, Lithography-based fabrication of nanopore arrays in freestanding SiN and graphene membranes, *Nanotechnology* **29**, 145302 (2018).
 - [3] A. Alizadeh, W.-L. Hsu, M. Wang, and H. Daiguji, Electroosmotic flow: From microfluidics to nanofluidics, *Electrophoresis* **42**, 834 (2021).
 - [4] K. Lee, K.-B. Park, H. J. Kim, J.-S. Yu, H. Chae, H.-M. Kim, and K.-B. Kim, Recent progress in solid-state nanopores, *Adv. Mater.* **30**, 1704680 (2018).
 - [5] M. Tsutsui, S. Hongo, Y. He, M. Taniguchi, N. Gemma, and T. Kawai, Single-nanoparticle detection using a low-aspect-ratio pore, *ACS Nano* **6**, 3499 (2012).

- [6] H. Daiguji, P. Yang, A. J. Szeri, and A. Majumdar, Electrochemomechanical energy conversion in nanofluidic channels, *Nano Lett.* **4**, 2315 (2004).
- [7] W.-L. Hsu and H. Daiguji, Manipulation of protein translocation through nanopores by flow field control and application to nanopore sensors, *Anal. Chem.* **88**, 9251 (2016).
- [8] M. M. Hatlo, D. Panja, and R. van Roij, Translocation of DNA molecules through nanopores with salt gradients: The role of osmotic flow, *Phys. Rev. Lett.* **107**, 068101 (2011).
- [9] M. Wanunu, T. Dadosh, V. Ray, J. M. Jin, L. McReynolds, and M. Drndic, Rapid electronic detection of probe-specific microRNAs using thin nanopore sensors, *Nat. Nanotechnol.* **5**, 807 (2010).
- [10] T. A. Zangle, A. Mani, and J. G. Santiago, Theory and experiments of concentration polarization and ion focusing at microchannel and nanochannel interfaces, *Chem. Soc. Rev.* **39**, 1014 (2010).
- [11] A. D. MacGillivray, Nernst-Planck equations and the electroneutrality and Donnan equilibrium assumptions, *J. Chem. Phys.* **48**, 2903 (1968).
- [12] E. J. F. Dickinson, J. G. Limon-Petersen, and R. G. Compton, The electroneutrality approximation in electrochemistry, *J. Solid State Electrochem.* **15**, 1335 (2011).
- [13] W.-L. Hsu, J. Hwang, and H. Daiguji, Theory of transport-induced-charge electroosmotic pumping toward alternating current resistive pulse sensing, *ACS Sens.* **3**, 2320 (2018).
- [14] Y. He, M. Tsutsui, R. H. Scheicher, C. Fan, M. Taniguchi, and T. Kawai, Mechanism of how salt-gradient-induced charges affect the translocation of DNA molecules through a nanopore, *Biophys. J.* **105**, 776 (2013).
- [15] X. Zhu, L. Guo, S. Ni, X. Zhang, and Y. Liu, Transport-induced inversion of screening ionic charges in nanochannels, *J. Phys. Chem. Lett.* **7**, 5235 (2016).
- [16] J. L. Anderson, Colloid transport by interfacial forces, *Annu. Rev. Fluid Mech.* **21**, 61 (1989).
- [17] D. C. Prieve, J. L. Anderson, J. P. Ebel, and M. E. Lowell, Motion of a particle generated by chemical gradients. Part 2. Electrolytes, *J. Fluid Mech.* **148**, 247 (1984).
- [18] H. J. Keh, Diffusiophoresis of charged particles and diffusioosmosis of electrolyte solutions, *Curr. Opin. Colloid Interface Sci.* **24**, 13 (2016).
- [19] A. Gupta, B. Rallabandi, and H. A. Stone, Diffusiophoretic and diffusioosmotic velocities for mixtures of valence-asymmetric electrolyte, *Phys. Rev. Fluids* **4**, 043702 (2019).
- [20] Z. Ulberg and A. Dukhin, Electrodiffusiophoresis - film formation in Ac and Dc electrical fields and its application for bactericidal coatings, *Prog. Org. Coat.* **18**, 1 (1990).
- [21] S. E. Yalcin, S. Y. Lee, S. W. Joo, O. Baysal, and S. Qian, Electrodiffusiophoretic motion of a charged spherical particle in a nanopore, *J. Phys. Chem. B* **114**, 4082 (2010).
- [22] Y.-C. Chung, J.-P. Hsu, and S. Tseng, Electrodiffusioosmosis in a solid-state nanopore connecting two large reservoirs: Optimum pore size, *J. Phys. Chem. C* **118**, 19498 (2014).
- [23] S. M. Davidson, M. B. Andersen, and A. Mani, Chaotic induced-charge electro-osmosis, *Phys. Rev. Lett.* **112**, 128302 (2014).
- [24] T. M. Squires and M. Z. Bazant, Induced-charge electro-osmosis, *J. Fluid Mech.* **509**, 217 (2004).
- [25] See Supplemental Material at <http://link.aps.org/supplemental/10.1103/PhysRevFluids.9.L071701> for numerical simulation details, justification of assumptions made in the analytical model, and derivation of Eq. (6).
- [26] J. H. Masliyah and S. Bhattacharjee, *Electrokinetic and Colloid Transport Phenomena*, 4th ed. (Wiley, New York, 2006).
- [27] C. Huang, P. Choi, K. Nandakumar, and L. Kostiuk, Comparative study between continuum and atomistic approaches of liquid flow through a finite length cylindrical nanopore, *J. Chem. Phys.* **126**, 224702 (2007).
- [28] Y. Ai, J. Liu, B. Zhang, and S. Qian, Field effect regulation of DNA translocation through a nanopore, *Anal. Chem.* **82**, 8217 (2010).
- [29] M. Mao, S. Ghosal, and G. Hu, Hydrodynamic flow in the vicinity of a nanopore induced by an applied voltage, *Nanotechnology* **24**, 245202 (2013).
- [30] D. J. E. Harvie, An implicit finite volume method for arbitrary transport equation, *ANZIAM J.* **52**, C1126 (2012).
- [31] J.-F. Geuzaine and C. Remacle, Gmsh: A 3-D finite element mesh generator with built-in pre and post-processing facilities, *Int. J. Numer. Methods Eng.* **79**, 1309 (2009).

- [32] Z. Wang, W.-L. Hsu, S. Tsuchiya, S. Paul, A. Alizadeh, and H. Daiguji, Joule heating effects on transport-induced-charge phenomena in an ultrathin nanopore, *Micromachines* **11**, 1041 (2020).
- [33] R. P. Bharti, D. J. E. Harvie, and M. R. Davidson, Steady flow of ionic liquid through a cylindrical microfluidic contraction/expansion pipe: Electroviscous effects and pressure drop, *Chem. Eng. Sci.* **63**, 3593 (2008).
- [34] E. V. Levine, M. M. Burns, and J. A. Golovchenko, Nanoscale dynamics of joule heating and bubble nucleation in a solid-state nanopore, *Phys. Rev. E* **93**, 013124 (2016).
- [35] A. Boika and A. S. Baranski, Dielectrophoretic and electrothermal effects at alternating current heated disk microelectrodes, *Anal. Chem.* **80**, 7392 (2008).
- [36] J. E. Hall, Access resistance of a small circular pore, *J. Gen. Physiol.* **66**, 531 (1975).
- [37] S. Paul, W.-L. Hsu, M. Magnini, L. R. Mason, Y.-L. Ho, O. K. Matar, and H. Daiguji, Single-bubble dynamics in nanopores: Transition between homogeneous and heterogeneous nucleation, *Phys. Rev. Res.* **2**, 043400 (2020).
- [38] A. Gadaleta, C. Sempere, S. Gravelle, A. Siria, R. Fulcrand, C. Ybert, and L. Bocquet, Subadditive ionic transport across arrays of solid-state nanopores, *Phys. Fluids* **26**, 012005 (2014).
- [39] F. Henrique, P. J. Zuk, and A. Gupta, Charging dynamics of electrical double layers inside a cylindrical pore: Predicting the effects of arbitrary pore size, *Soft Matter* **18**, 198 (2022).
- [40] V. Levadny, V. M. Aguilera, and M. Belaya, Access resistance of a single conducting membrane channel, *Biochim. Biophys. Acta* **1368**, 338 (1998).
- [41] W.-L. Hsu, D. J. E. Harvie, M. R. Davidson, D. E. Dunstan, J. Hwang, and H. Daiguji, Viscoelectric effects in nanochannel electrokinetics, *J. Phys. Chem. C* **121**, 20517 (2017).
- [42] W.-L. Hsu, D. Harvie, M. Davidson, H. Jeong, E. Goldys, and D. Inglis, Concentration gradient focusing and separation in a silica nanofluidic channel with a non-uniform electroosmotic flow, *Lab Chip* **14**, 3539 (2014).
- [43] Z.-Y. Zhang, H.-L. Cui, D.-P. Huang, and D.-Q. Wang, Single nucleotide discrimination with sub-two nanometer monolayer graphene pore, *Sens. Actuators B Chem.* **349**, 130792 (2021).
- [44] J. Feng, M. Graf, K. Liu, D. Ovchinnikov, D. Dumcenco, M. Heriranian, V. Nandigana, N. Aluru, A. Kis, and A. Radenovic, Single-layer MoS₂ nanopores as nanopower generators, *Nature (London)* **536**, 197 (2016).
- [45] S. H. Lee and J. C. Rasaiah, Molecular dynamics simulation of ionic mobility. I. Alkali metal cations in water at 25 °C, *J. Chem. Phys.* **101**, 6964 (1994).
- [46] S. Kerisit, M. Vijayakumar, K. S. Han, and K. T. Mueller, Solvation structure and transport properties of alkali cations in dimethyl sulfoxide under exogenous static electric fields, *J. Chem. Phys.* **142**, 224502 (2015).
- [47] G. N. Watson, *A Treatise on the Theory of Bessel Functions*, 2nd ed. (Cambridge University Press, Cambridge, UK, 1966).
- [48] M. Mao, J. Sherwood, and S. Ghosal, Electro-osmotic flow through a nanopore, *J. Fluid Mech.* **749**, 167 (2014).
- [49] R. Mancinelli, A. Botti, F. Bruni, M. A. Ricci, and A. K. Soper, Hydration of sodium, potassium, and chloride ions in solution and the concept of structure maker/breaker, *J. Phys. Chem. B* **111**, 13570 (2007).